ACADEMIC PRESS

Available online at www.sciencedirect.com
SCIENCE DIRECT®

Journal of Catalysis 219 (2003) 74–84

JOURNAL OF CATALYSIS

www.elsevier.com/locate/jcat

Structure, morphology, and catalytic activity of β zeolite synthesized in a fluoride medium for asymmetric hydrogenation

Q.-H. Xia,[a,*] S.-C. Shen,[b] J. Song,[b] S. Kawi,[b] and K. Hidajat [b]

[a] *Chemical and Process Engineering Centre, National University of Singapore, Block E5 Basement 08, Singapore*
[b] *Department of Chemical and Environmental Engineering, National University of Singapore, Singapore*

Received 25 September 2002; revised 2 December 2002; accepted 12 March 2003

Abstract

A series of beta (β) zeolites has been synthesized in a fluoride medium and characterized by different techniques. XRD showed that the majority of F–Si–β, F–Pt–β, F–Pd–β, and F–W–β materials consisted of polymorph A. W and Al were incorporated into the framework of β, while Pt and Pd existed on the surface of β in the form of PtO_x or PdO_x oxides. The framework structures of F–Si–β, F–Pt–β, and F–Pd–β were almost identical, as proven by ^{29}Si MAS NMR and FTIR spectra. The relative coverage of surface –OH groups decreased in the sequence H–β > H–ZSM-5 > F–Al–β > F–W–β > F–Pd–β > F–Pt–β > F–Si–$\beta(1)$ > F–Si–$\beta(2)$. SEM revealed an especially uniform crystalline morphology of F–Si–$\beta(2)$ nucleated spontaneously and a mixed morphology of F–Si–$\beta(1)$, F–W–β, F–Pt–β, and F–Pd–β induced by seeding H–β. The reduced F–Pt–β and F–Pd–β were catalytically active for the asymmetric hydrogenation of tiglic acid with an appreciable enantiomeric excess value of about 9–11% without adding chiral modifiers.

Keywords: Beta zeolite; Fluoride medium; Chiral β structure; Control of morphology; Spontaneous nucleation; Chiral hydrogenation; Tiglic acid

1. Introduction

Zeolites constitute an important class of catalysts and are finding wide application in the petrochemical and fine chemical industries. Beta (β) zeolite is the only high-silica zeolite possessing a three-dimensional system of large rings (rings of 12 oxygen atoms as the minimum constricting apertures) [1,2]. This gives β zeolite interesting potential applications in acid-catalyzed reactions where high thermal and hydrothermal stability and low steric restrictions can be of paramount importance [3–5]. Much effort has been devoted to the synthesis of commercially important beta zeolite since beta zeolite is of great potential industrial interest as a good catalyst for many reactions [6–12]. Another reason for the interest in β zeolite is the possibility of synthesizing a chiral, enantiomerically pure zeolite and the potential applications of such a catalyst in enantioselective reactions. β zeolite is an intergrowth of two (or three) polymorphs (A, B, and C), one of them (polymorph A) being the only known real zeolite structure showing chirality [1,2]. Certainly its small pore diameter ($\sim$ 7 Å) limits its effectiveness with only small molecule compounds.

The isomorphous substitution of aluminum in the beta zeolite framework by other elements such as iron [13,14], boron [15], indium [16], gallium [17,18], or titanium [19] has been achieved by direct synthesis from alkaline reaction media or by a dry-gel conversion technique. By using a near-neutral nonalkaline medium, where hydroxide anions are replaced by fluoride anions as the mineralizing agent, the (Si, Al) and (Si, B) beta zeolites were prepared in the presence of 1,4-diazabicyclo [2,2,2] octane (Dabco) and methylamine as the templates [20,21]. From similar almost neutral fluoride-containing media, the synthesis of pure silica (Si, Ti), (Si, Al), and (Si, Ga) beta zeolites was also reported in the presence of tetraethylammonium cations as the structuring agent [22–25].

The framework structure of β zeolite prepared from a fluoride medium has been suggested to be chiral, as polymorph A is predominantly different from conventional β zeolite. Beta zeolite obtained shows a much better resolution of the diffraction peaks and this is probably a consequence not only of its large average crystal size (0.5–5 μm well-faceted truncated square bipyramids) but also of its defect-free nature

* Corresponding author.
E-mail address: xia1965@yahoo.com (Q.-H. Xia).

0021-9517/$ – see front matter
doi:10.1016/S0021-9517(03)00154-4

[22,25]. Features appearing in the XRD pattern calculated using the proposed faulted model, which usually are not well resolved in the experimental patterns, are clearly distinguished in these beta materials. Interestingly, the shoulder at the low-angle side in the first low-angle peak suggests in the material the stacking probability is lower than the usual 0.6 value; i.e., the material is nearer to polymorph A than to polymorph B [22]. The experimental results match very well the simulated structure of polymorph A. ^{29}Si MAS NMR has ascertained the absence of connectivity defects in such a high-silica β zeolite as only Si (4Si) resonances appear.

The majority of heterogeneously catalyzed enantioselective hydrogenations used to focus on Pt or Pd-containing Al_2O_3, SiO_2, or active carbon catalysts for the conversion of some substrates [26–29]. There were also some successful uses of Pt-containing zeolitic catalysts, such as types Y, ZSM-5, ZSM-35, and beta, for enantioselective reactions [29,30]. However, to control the enantioselectivity of the products, an auxiliary chiral modifier like (+)-cinchonine, (−)-cinchonidine, (−)-proline, etc. had to add into the reaction mixtures; without the chiral modifier only one racemic mixture could be obtained [26–32]. Due to the special chiral structure, β zeolite prepared from a fluoride medium is worthy of being researched as a catalyst for chiral hydrogenation. However, to date no study on this system has been reported in the literature. In the present work, we report the synthesis of siliceous (Si, Al), (Si, W), (Si, Pt), and (Si, Pd) beta zeolites in a fluoride medium and the effect of seeding and synthesis route on the morphology of various β zeolite crystals. The activity and enantioselectivity of as-synthesized F–Pt–β and F–Pd–β catalysts for the hydrogenation of tiglic acid was first investigated.

2. Experimental

2.1. Synthesis

The raw materials used were TEOS (tetraethyl orthosilicate, 98%, Aldrich), TEAOH (tetraethyl ammonium hydroxide, 35 wt% in water, Aldrich), hydrofluoric acid (40 wt% HF, Aldrich), $Pt(NH_3)_4(NO_3)_2$ (98%, Aldrich), $Pd(NO_3)_2$ (97%, Aldrich), $(NH_4)_2WO_4$ (99%, Aldrich), aluminum powder, $NaAlO_2$, KCl, NaOH, aerosil-200 silica, NH_4NO_3, and deionized water. NaZSM-5 ($Si/Al = 25$) and NaY ($Si/Al = 4.7$) were commercial products. Other chemicals used were methanol (99.8%, redistilled), *S*-(+)-α-methylbutyric acid (98%), *R*-(−)-α-methylbutyric acid (97%), and tiglic acid (98%).

2.2. H–β

The mixture of 120 g of 20 wt% TEAOH solution, 2.2267 g of $NaAlO_2$, 0.90 g of KCl, and 0.15 g of NaOH was stirred until it became a transparent solution. Then 32.59 g of aerosil-200 silica was added. The resulting homogeneous sol was transferred into a Teflon-lined stainless-steel autoclave and heated to 170 °C statically. After 40 h, the autoclave was quenched, the content filtered, and the solid washed with deionized water. After drying at 96 °C overnight, the solid was calcined at 540 °C for 20 h. The resultant white solid Na–Al–β was ion-exchanged with 20 wt% of NH_4NO_3 solution at 60 °C three times into NH_4-Al–β. Each time, 1 g of Na–Al–β was stirred with 25 ml of NH_4NO_3 solution at 60 °C for 3 h. Finally, NH_4–Al–β was decomposed into H–β at 500 °C for 3 h. H–ZSM-5 ($Si/Al = 27.5$) and H–Y ($Si/Al = 6.7$) was prepared by using the same ion-exchange procedure and recalcination.

2.3. F–Al–β, F–Pt–β, F–Pd–β, F–W–β

The mixture of 21.8 g of 35 wt% TEAOH solution, 20.4 g of 98 wt% TEOS, 4 g of water, and the compounds containing Al (0.4 g of Al powder), Pt (6.0 ml of 0.05 M $Pt(NH_3)_4(NO_3)_2$ solution), Pd (3.0 ml of 0.1 M $Pd(NO_3)_2$ solution), or W (0.4 g of $(NH_4)_2WO_4$) was stirred overnight at room temperature to become a homogeneous sol. Thereafter, about 0.40 wt% of H–β seeding powder was added into the precursor sol of F–Pt–β, F–Pd–β, and F–W–β under vigorous stirring to accelerate the crystallization, and the stirring was kept for another 2 h. Then 2.7 g of HF solution was added dropwise into the sol under vigorous stirring. The resulting gel was crashed and transferred into a Teflon-lined stainless-steel autoclave. The crystallization was statically carried out at 140 °C for 12 days for F–Al–β and for 6 days for the other samples. After that, the autoclave was quenched, the content filtered, and the solid washed with deionised water. After being dried at 96 °C overnight, the solid was calcined at 550 °C for 8 h. Note that F–Pt–β and F–Pd–β were pre-reduced in a flow of pure hydrogen at 400 °C for 10 h prior to catalytic tests, and the respective dispersion of metal Pt or Pd (active species) on β was 65% or 69%.

2.4. F–Si–β

The mixture of 21.8 g of 35 wt% TEAOH solution, 20.4 g of 98 wt% TEOS, and 4 g of water was stirred overnight at room temperature to become a homogeneous sol. In the synthesis of F–Si–$\beta(1)$, about 0.39 wt% of H–β seeding powder was added to the precursor sol and stirred for another 2 h before 2.7 g of HF solution was added dropwise. In the synthesis of F–Si–$\beta(2)$, to the resultant sol merely 2.7 g of HF solution was added together without seeding. The subsequent procedures were similar to those described in the former text, in which F–Si–$\beta(1)$ and F–Si–$\beta(2)$ were crystallized at 140 °C for 6 and 12 days, respectively. EDX determination showed that the Si/Al ratio in two siliceous beta crystals was more than 5000.

2.5. Impregnation of Pd-supported catalysts

Pd-supported catalysts with a PdO loading of 0.64 wt% (Si/Pd = 316.7) were prepared through an impregnation method as follows: 2 g of powder supports (HZSM-5, H–β, and H–Y) pre-dried at 300 °C overnight were added into a certain amount of 0.1 M $Pd(NO_3)_2$ solution and the mixture was vigorously stirred at room temperature for 24 h. Then the suspension was dried at 60 °C overnight, followed by calcinations at 550 °C for 10 h in a flow of air. Prior to catalytic tests, these catalysts were pre-reduced in a flow of pure hydrogen at 400 °C for 10 h, and the dispersion of Pd metal on three catalysts was determined to be 35% for Pd/HZSM-5, 48% for Pd/H–β, and 57% for Pd/H–Y, respectively.

2.6. Characterization of catalysts

All of the solids (calcined) were characterized by a Shimadzu XRD-6000 X–ray diffractometer using Ni-filtered Cu-K_α radiation operating at 40 kV/30 mA. The scanning range was $2\theta = 3$–$60°$ or $2\theta = 5$–$10°$. The relative crystallinity was evaluated by comparing the area of the characteristic peaks ($2\theta = 7.7°$, $22.5°$) of the solid product with that of the reference sample F–Si–$\beta(1)$ induced by seeding H–β in a fluoride medium. Autosorb-1 was used to determine the N_2 adsorption–desorption isotherms of the samples. Prior to the measurements, the samples were degassed at 300 °C overnight. The BET-specific surface area was calculated using the BET equation in the range of relative pressures between 0.05 and 0.25. The BJH method was used to calculate the pore volume and pore size distribution of the samples.

A Simadzu FTIR-8700 Fourier transform infrared spectrophotometer was used to determine the framework vibrations of beta zeolites. The mixture of KBr and sample solid powder (200:1) was carefully ground and pressed into a round wafer under a pressure of 5 t cm^{-2}. The framework vibrational spectra were recorded between 400 and 4000 cm^{-1} with a resolution of 4 cm^{-1}.

The FTIR spectra of surface hydroxyl groups were recorded using a Shimadzu FTIR-8700 Fourier transform infrared spectrophotometer having a resolution of 2 cm^{-1} and connected to a PFEIFFER vacuum system. Before scanning, a self-supporting round wafer (20 mg, with a pressure of 6 t cm^{-2}) of the sample was evacuated at 350 °C for 5 h in an IR cell under a residual pressure of 10^{-6} mbar. The relative coverage of surface hydroxyl groups of the samples was evaluated by comparing the integrated area of the hydroxyl bands (3000–3750 cm^{-1}) to that of the H–β zeolite.

The morphology of crystalline materials was observed using a JEOL JSM-5600LV scanning electron microscope under vacuum at 10^{-6}–10^{-7} mbar. The siliceous sample must be coated with Pt sputtering prior to the determination. The average size of crystal particles was calculated according to SEM pictures. Scanning electron microscope-energy-dispersive X-ray (SEM-EDX) analysis was also conducted on the JEOL JSM-5600LV scanning electron microscope using a silicon detector operating at an accelerating voltage of 15 kV and a beam current of 1.0 nA under vacuum at 10^{-6}–10^{-7} mbar. The element used for optimization was copper, and all quantitative results below 2σ were set to zero.

^{29}Si MAS NMR spectra were obtained at 300 K with a Bruker FT NMR, DRX-400 MHz instrument operating at 79.46 MHz and 35 s of recycle delays. The chemical shift of ^{29}Si (in ppm) was based on the external $Si(CH_3)_4$ as a reference. ICP elemental analysis was performed with a Perkin-Elmer Optima 3000DV spectrometer. Calibration standards with different concentrations were prepared by diluting the corresponding standard metal solutions. Pt or Pd metal dispersion on β was determined by equilibrium hydrogen chemisorption at room temperature in AUTOSORB-6B (Quantachrome). Prior to H_2 adsorption analysis, the samples were evacuated at 200 °C for 1 h, exposed to static H_2 at 300 °C for 2 h, and placed under dynamic vacuum at 300 °C for 3 h [33].

2.7. Catalytic hydrogenation

In a glove box under a nitrogen atmosphere, a 150-ml stainless-steel Parr reactor was charged with 200 mg of powder catalyst (pre-dried at 180 °C in a vacuum oven overnight) and 168 mg of tiglic acid for hydrogenation. To the reactor was added 32 ml of methanol as the solvent. The reactor was then closed and pressurized to 13.8–55.2 bar H_2 pressure and stirred for 10 h at room temperature. After 10 h, the solid powder of catalyst F–Pd–β was filtered to separate it from the reaction mixture liquid, washed several times with methanol, dried at 180 °C in a vacuum oven overnight, and then re-used in the next reaction (H_2 pressure: 27.6 bar). Note that in one run 200 mg of Pd/H–ZSM-5 was used as the catalyst, while 300 mg of siliceous F–Si–β was added as the modifier. The conversion (mol%) and e.e. (%) (enantiomeric excess) of products was determined by a HP-6890 series gas chromatograph equipped with an FID and a CP-Chirasil-L-VAL capillary column where H_2 was used as the carrier gas. The hydrogenised products were R-(−)- and S-(+)-α-methylbutyric acids, and the appearance of GC peaks was observed in the following sequence: methanol, S-(+)-α-methylbutyric acid, R-(−)-α-methylbutyric acid, and tiglic acid, where the retention time was calibrated by syringing a solution of each standard compound in methanol into the GC system. The e.e. (%) value was calculated to be equal to $(S_R - S_S)/(S_R + S_S) \times 100\%$, where S_R and S_S stand for the respective selectivity of R-(−)- and S-(+)-enantiomers. TON (turnover number) characterizing the activity of catalyst was equal to (moles of products)/(moles of metal Pt or Pd in the catalysts). GC error for the determination of e.e. (%) value was within ±2%.

Table 1
Synthesis parameters, crystallinity, and compositions of all zeolite samples

Sample	Seeding[a] (wt%)	Time (d)	Temp. (°C)	Crystallinity[b] (%)	Si/M molar ratio[c] Gel	Product
F–Si–β(1)	0.39	6	140	100	∞	> 5000[d]
F–Si–β(2)	0	12	140	103	∞	> 5000[d]
F–Pt–β	0.40	6	140	138	317.0	321.3
F–Pd–β	0.40	6	140	139	314.4	319.6
F–W–β	0.39	6	140	94	69.1	64.3
F–Al–β	0	12	140	76	6.4	6.6
H–β	0	(40 h)	170	75	20.2	30.6
H–ZSM-5	–[e]	–[e]	175	–[e]	–[e]	27.5
H–Y	–[e]	–[e]	100	–[e]	–[e]	6.7

[a] H–β powder as seeding crystals.
[b] The relative crystallinity (%) is evaluated by comparing the area of the main peaks ($2\theta = 7.7°$, 22.5°) of the solid product with that of the reference sample F–Si–β(1).
[c] M stands for metals such as Al, Pt, Pd, or W, and Si/M ratio is calculated based on ICP analysis.
[d] Si/M ratio is calculated based on EDX determination.
[e] Not determined.

3. Results and discussion

3.1. Characterization of structure of beta zeolites

In our study, TEAOH was used as the base and the structure-directing agent to template the formation of β framework in a fluoride medium. When TMAOH was used to replace TEAOH as the base and template, the solid was always amorphous. When HS-40 silica sol, NaOH, and TEACl were used as raw materials, even if the seeding crystals (H–β) were added, the recovered solid was still amorphous. In the synthesis of F–Al–β, the Al source was AlF_6^{3-} anions coming from the reaction between Al powder and F^- anions. Table 1 lists the synthesis parameters, crystallinity, and compositions (ICP or EDX analysis) of all samples, where the respective Si/M ratio in the products was Si/Al = 30.6 for H–β, Si/Al = 6.6 for F–Al–β, Si/W = 64.3 for F–W–β, Si/Pt = 321.3 for F–Pt–β, and Si/Pd = 319.6 for F–Pd–β. EDX determination shows that the Si/M ratio in F–Si–β(1) and F–Si–β(2) was > 5000, indicative of their siliceous nature. When the area under the main peaks ($2\theta = 7.7°$, 22.5°) is compared to the standard highly crystalline zeolite F–Si–β(1) (induced by seeding H–β in a fluoride medium), the relative crystallinities from 75 to 139% are obtained for all crystalline solids. XRD patterns in Fig. 1 show that the solids, except for the bottom one, are highly crystalline β zeolite. Features appearing in the XRD patterns calculated using the proposed faulted model [1,22], which usually are not well resolved in the experimental patterns, are clearly distinguished in almost all solids except H–β and F–Al–β with a low Si/Al ratio of 6.6. As shown in Fig. 2, a clear strong peak appears at the low-angle side (about 7.08° 2θ) in the first low-angle peak (about 7.68° 2θ) for F–Si–β, F–Pt–β, F–Pd–β, and F–W–β, while for F–Al–β this peak becomes an ambiguous shoulder peak and shifts to about 7.18° (2θ); however, the same peak cannot be observed for H–β at all. This suggests that the stacking probability (as defined in

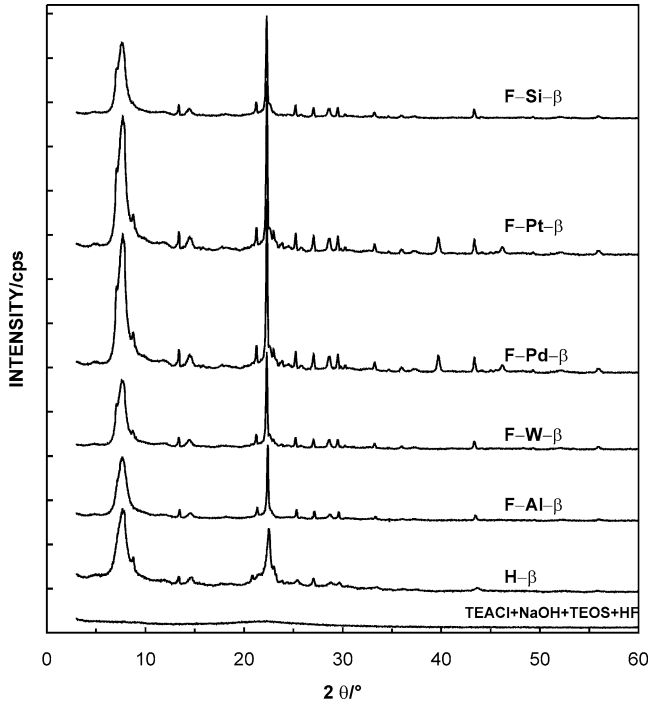

Fig. 1. XRD patterns of beta samples and amorphous phase synthesized in a fluoride medium.

Ref. [22]) in the F–Si–β, F–Pt–β, F–Pd–β, and F–W–β materials is lower than the usual value of 0.6; i.e., the majority of these materials consist of polymorph A with chiral structure, consistent with the observations reported in [22,25]. The results show that F–Si–β, F–Pt–β, F–Pd–β, and F–W–β materials are constituted of chiral porous channels. Note that the peak at about 8.8° 2θ in the X-ray spectra of some samples may be ascribed to the appearance of crystalline impurities such as ZSM-5 or ZSM-12 (< 5%). As compared with the other samples, two clear diffraction peaks at 39.8° and 46.4° 2θ appear in the XRD patterns of F–Pt–β and F–Pd–β. Obviously, these two peaks should be assigned to the

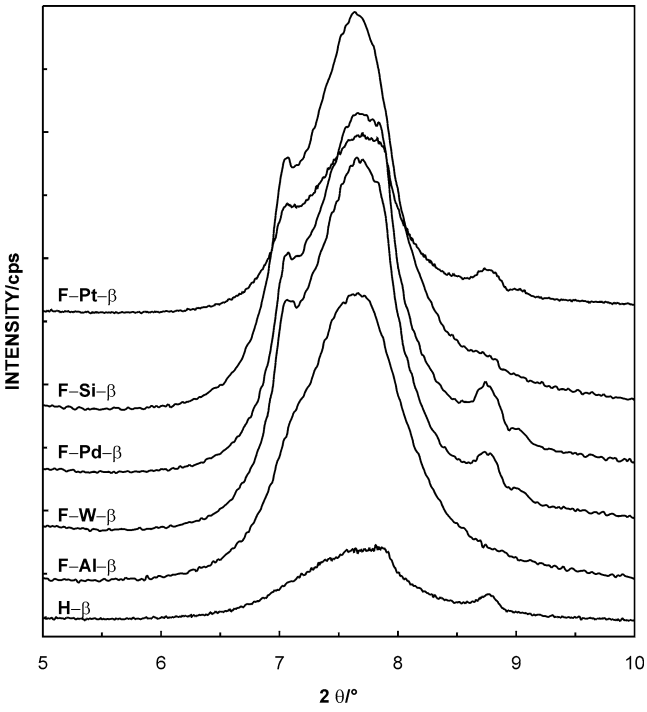

Fig. 2. Comparison of characteristics of X-ray diffraction at a low angle of various beta zeolites.

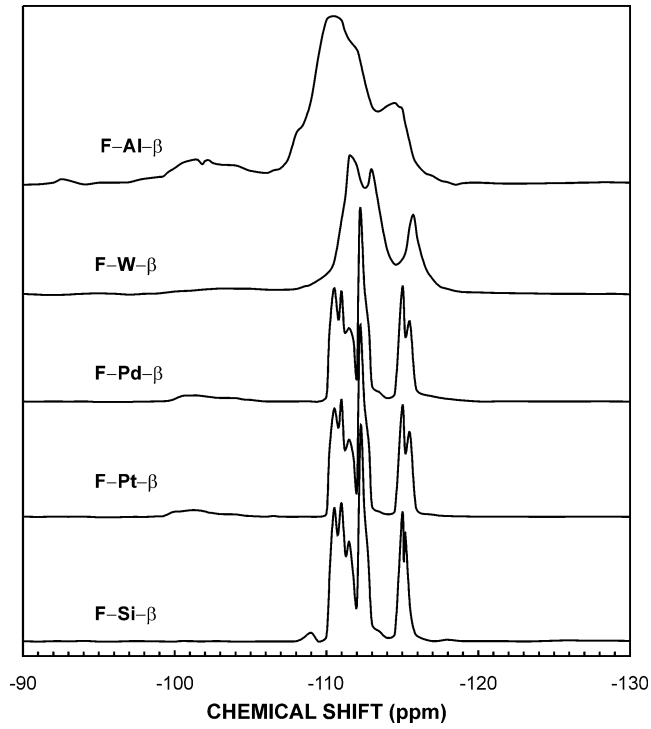

Fig. 3. ^{29}Si MAS NMR spectra of different beta zeolites.

existence of PtO_x and PdO_x on the surface of β. The results show that noble metals Pt and Pd were not incorporated into the framework lattice of zeolites, while W and Al were introduced into the frameworks of zeolites, further proven by the fact that after calcinations, colorless F–Al–β and F–W–β, grey F–Pt–β, and brown F–Pd–β were obtained. Once F–Pt–β and F–Pd–β were reduced in the flow of hydrogen, PtO_x and PdO_x were converted to black Pt and Pd metals dispersed on β, which are active species in the hydrogenation. The addition of metal precursors during the synthesis of F–Pt–β and F–Pd–β actually led to a good dispersion of noble metals Pt and Pd in the chiral pores in which the determined dispersion was 65% for Pt or 69% for Pd, higher than 48% on Pd/H–β prepared by impregnation. However, high Al content in a fluoride medium and in a conventional alkaline medium led to a mixed phase of polymorphs A, B, and C without chirality, as exhibited by the XRD patterns of the F–Al–β and H–β samples, in which only an ambiguous shoulder was observed at the low-angle side of about 7.08° 2θ.

The incorporation of W and Al into the framework of β seriously affected the resolution of crystallographic tetrahedral sites in the products as well, as shown in Fig. 3. The chiral β zeolite structure has been proven to be free of connectivity defects in these materials by ^{29}Si MAS NMR, while a great concentration of these defects is detected in the conventional samples [22,34,35]. The literature reported that for siliceous β zeolite synthesized in a traditional hydroxide medium, there were two resonances in the ^{29}Si MAS NMR spectrum, one of which located at about −110.9 ppm assigned to Q^4 sites and the other appearing at −101.6 ppm assigned to Q^3 sites [5,15]. The formation of Q^3 was assumed to originate from structural defects ($Si–O^-$ or Si–OH groups), necessary for counterbalancing the charge of TEA^+. However, for siliceous β zeolite synthesized in a fluoride medium only Q^4 resonances at −110 to −117 ppm appeared in the ^{29}Si MAS NMR spectrum, and nine different crystallographic tetrahedral sites were resolved [22,25,36]. As can be observed in Fig. 3, the spectrum of calcined F–Si–$\beta(2)$ is similar to that reported in the literature and shows well-resolved lines in the range of −108.5 to −116.5 ppm corresponding to Q^4 species ($–Si(OSi)_4$) occupying more than seven different crystallographic tetrahedral sites, which ascertains the absence of connectivity defects in this sample [22,25]. Compared with those of F–Si–$\beta(2)$, the spectra of calcined F–Pt–β and F–Pd–β show obvious broadening of the lines and a weak broad resonance appears in the −99 to −104 ppm range, corresponding to a low concentration of Q^3 sites, possibly ascribed to the negative effect of PtO_x or PdO_x oxides on the crystallization. For the calcined F–W–β, the tendency of broadening of the lines in the range of −110 to −117 ppm remarkably intensifies, where about three to four different crystallographic sites are resolved; a weak broad resonance appears in the −100 to −108 ppm range assigned to the formation of ($–Si(OSi)_3(OW)_1$) or ($–Si(OSi)_3(OH)_1$) defects due to the incorporation of W into the framework of β. Along with the incorporation of Al into the framework of F–Al–β, only two strong broad resonances at −110.5 and −115.0 ppm and two weak shoulder peaks at −108 and −112 ppm are observed in the range of resonances corresponding to Q^4 sites. Additionally, two clear broad resonances appear in the −100 to −108 ppm range as well,

Table 2
BET surface area, pore volume, surface –OH relative coverage, and crystal size of β zeolites and ZSM-5 zeolite

Sample	BET surface area (m^2/g)	Pore volume (cm^3/g)	–OH relative coverage (%)	Crystal size (μm)
F–Si–β(1)	628.9	0.32	27.8	1–4
F–Si–β(2)	587.9	0.30	23.7	7–15
F–Pt–β	535.0	0.28	33.9	1–4
F–Pd–β	556.3	0.28	37.4	1–4
F–W–β	535.9	0.28	45.9	1.5–3.5
F–Al–β	506.5	0.28	47.3	8–16
H–β	650.4	0.35	100	0.3–1
H–ZSM-5	440.9	0.24	55.8	0.5–1.2
H–Y	735.4	0.42	n.d.	0.5–2

–OH relative coverage (%) is evaluated by comparing the integrated area of the hydroxyl bands (3000–3750 cm^{-1}) to that of the H–β zeolite; n.d.: not detected.

indicative of an increase of density of connectivity defects in F–Al–β. Based on the observations with XRD and ^{29}Si MAS NMR, we can come to the conclusion that, in the case of F–Pt–β and F–Pd–β, pure silica beta frameworks with high crystallinity were formed and large particles of PtO_x and PdO_x were present on the surface of these crystals.

Table 2 shows that the BET surface area and the pore volume of all β zeolites are much larger than those of ZSM-5, which is consistent with the differences in their pore diameters. The BET surface area and pore volume of all β samples decrease in the following order: H–β > F–Si–β(1) > F–Si–β(2) > F–Pd–β > F–Pt–β ≈ F–W–β > F–Al–β. The small crystal size with 0.3–1 μm determined by SEM made a big contribution to the large BET surface area of H–β zeolite, while the big crystal size with 8–16 μm resulted in the low BET surface area of F–Al–β. However, for other β samples synthesized in a fluoride medium it is difficult to correlate the BET surface area with their crystal sizes. It should be pointed out that the yield of the H–β sample (based on silica) was only about 70 wt%; however, for all fluorinated β zeolites, that was larger than 95 wt%. It means that amorphous phase in small amounts might still be contained in some samples synthesized from a fluoride medium, further decreasing the BET surface area and pore volume of the samples. In addition, the BET surface area and pore volume of H–ZSM-5 and H–Y are determined to be 440.9 m^2/g (0.24 cm^3/g) and 735.4 m^2/g (0.42 cm^3/g).

The change in the shape of N_2 adsorption–desorption isotherms for H–ZSM-5, H–β, and all β samples synthesized in a fluoride medium is depicted in Fig. 4. Clearly, all samples display *type I* isotherms, which is a typical characteristic of microporous solids [37]. The hysteresis loop of the H–β sample was not detected by our method, which could be associated with the morphology consisting of uniform, round, small crystals (0.3–1 μm). For all other samples, a *type H4* hysteresis loop was observed on the isotherms of these samples at a relative pressure higher than $p/p_0 = 0.45$. The *type H4* hysteresis loop is often associated with phase transitions of nitrogen, but in the case of *type I* isotherm

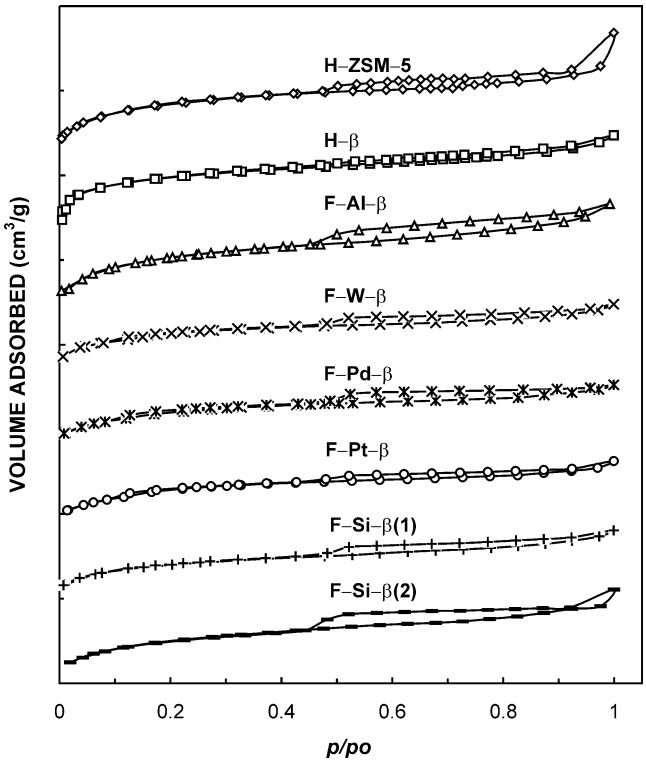

Fig. 4. Nitrogen adsorption–desorption isotherms of various zeolites.

character is indicative of microporosity [37]. The appearance of a *type H4* hysteresis loop on the isotherms of microporous ZSM-5 (∼ 5.5 Å) and β (∼ 7.0 Å) materials, resulting from the poor uniformity of crystal size distribution, can be ascribed to the contribution of capillary condensation of N_2 in interparticles or in agglomerates. As expected, the BJH pore diameter distributions (calculated based on the adsorption branch) of H–ZSM-5, H–β, F–Al–β, F–Si–β(1), and F–Si–β(2) were determined to be smaller than 10 Å, typical of microporous solids, as shown in Fig. 5. However, for F–W–β, F–Pt–β, and F–Pd–β a visible mesoporous size distribution is centered at 17.4–17.9 Å. Since a mesoporous inflection was not distinctly observed on the isotherms of these samples, therefore, the appearance of mesoporous size distribution cannot be assigned to the formation of regular mesopores in the solids but could be ascribed to the contribution of irregular mesoporous interparticulate void space [38].

The infrared spectra in Fig. 6 show that the vibration bands ranging from 350 to 1300 cm^{-1} of F–Si–β, F–Pt–β, F–Pd–β, and F–W–β frameworks are quite distinctly resolved. For F–Pt–β and F–Pd–β samples, about 18 framework vibration bands appeared at 354.9, 374.1, 426.3, 459.0, 474.5, 524.6, 576.7, 623.0, 642.3, 667.3, 677.0, 736.8, 775.3, 790.8, 808.1, 825.5, 1105.1, 1238.2 cm^{-1}; however, the weak vibration at about 355 cm^{-1} was invisible for F–W–β and F–Si–β. The visible vibration bands of F–Si–β, F–Pt–β, F–Pd–β, F–W–β, and F–Al–β are more than those of H–β. In contrast, the bands at 355, 667, 677, 737, 775, 808, and 825 cm^{-1} cannot be observed at all for H–β, while for F–Al–β only three bands at 355, 667, and 677 cm^{-1} are

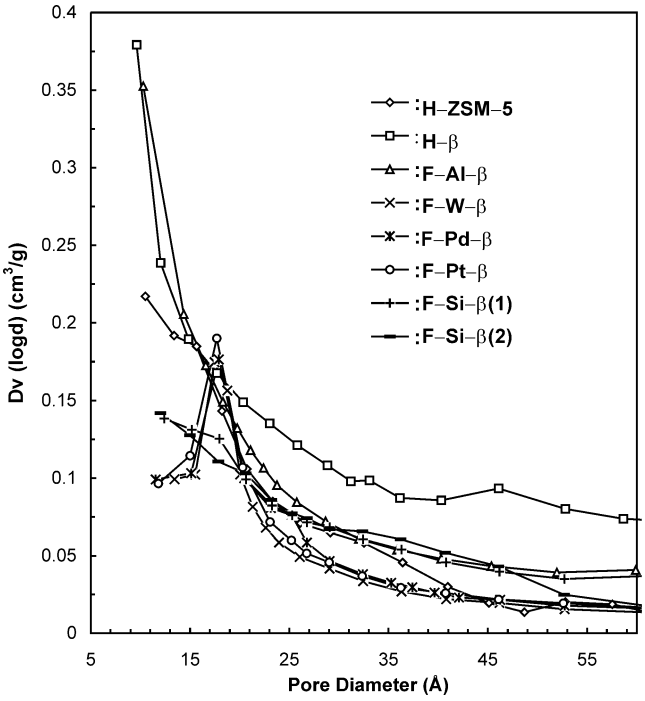

Fig. 5. Nitrogen adsorption pore size distribution of various zeolites.

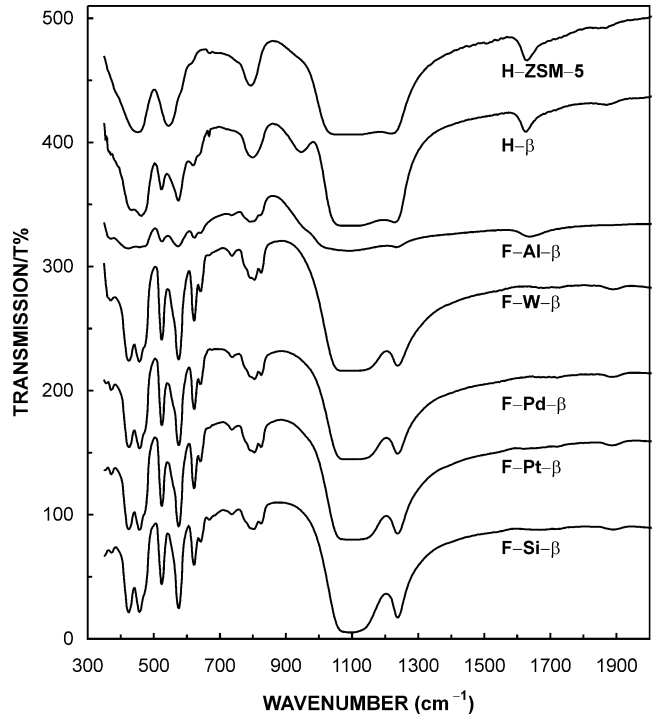

Fig. 6. IR vibration spectra of frameworks of various zeolites.

invisible. It means that synthesis in a fluoride medium can result in a higher resolution of all vibration environments of framework elements. This also shows that the incorporation of Al into β framework in either a fluoride medium or a non-fluoride medium largely decreases the number of oscillators locating in different vibration environments. In Ref. [39], the IR vibration modes from 300 to 1250 cm^{-1} have been, respectively, assigned to asymmetric stretching vibration mode (950–1250 cm^{-1}), to symmetric stretching vibration mode (650–820 cm^{-1}), to T–O bending vibration (300–650 cm^{-1}). The weak band at about 355 cm^{-1} for F–Pt–β, F–Pd–β, and F–W–β may be related to the vibration of weak mesopores consisting of interparticle void space. Fig. 6 also shows that the skeletal vibrations of β zeolite are totally different from those of ZSM-5 zeolite, which is because the frameworks of ZSM-5 and β zeolites are, respectively, consisting of different structural units. In particular, the vibration of terminal Si–OH at about 947 cm^{-1}, which is very strong for the H–β sample, cannot be observed at all for F–Si–β, F–Pt–β, F–Pd–β, and F–W–β; however, that becomes a small shoulder band and shifts to about 948 cm^{-1} for ZSM-5 and F–Al–β. This shows that there is a much higher concentration of hydroxyl groups on H–β than on other zeolites, further indicating that there is plenty of defects of connectivity on H–β [22].

3.2. Surface –OH relative coverage

FTIR spectra between 4000 and 2500 cm^{-1} of H–β, H–ZSM-5, and all β zeolites synthesized in a fluoride medium are shown in Fig. 7. In the present work, the H–β sample exhibits clear strong absorbance bands at about 3731.7, 3615.8, and 3536.7 cm^{-1} and shoulder bands at about 3691.1, 3683.4, 3660.2, 3575.3, 3559.8, and 3457.5 cm^{-1}. For H–ZSM-5, only about five absorbance bands with weak intensity are observed to locate at about 3733.6, 3714.3, 3683.4, 3621.6, and 3525.0 cm^{-1}, respectively. These respective hydroxyls were assigned to isolated silanols, locating in the region 3730–3742 cm^{-1}, and to associated hydroxyls with bridging OH bands in the region 3685–3600 cm^{-1} [40]. As we know, the framework of β nucleates and grows in a more difficult manner than that of ZSM-5 in the alkaline medium, resulting in the increase of surface defects of connectivity on H–β [3,19]. As compared with H–β, the relative coverage of surface –OH on all β zeolites synthesized in a fluoride medium showed a drastic reduction, especially for the isolated –OH absorbance band at 3733 cm^{-1}, as shown in Fig. 7. The F–Al–β sample exhibits more hydroxyl bands, at about 3733.6, 3691.1, 3679.5, 3656.4, 3633.2, 3598.4, 3579.2, 3563.7, 3540.5, 3517.4, and 3457.5 cm^{-1}, while for F–Si–β, F–Pt–β, and F–Pd–β these hydroxyl bands weaken and become ambiguous.

Table 2 shows the relative coverage of surface –OH on all samples, which has been calculated as a relative area fraction percentage (%). The relative coverage of surface –OH on different zeolite materials varies rather remarkably, which gradually reduces in the following sequence: H–β > H–ZSM-5 > F–Al–β > F–W–β > F–Pd–β > F–Pt–β > F–Si–$\beta(1)$ > F–Si–$\beta(2)$. The relative coverage of surface –OH on F–Al–β, F–W–β, and F–Pd–β is nearly 37–47% of that on H–β, whereas that on F–Pt–β and F–Si–β drops to about 34% and 24–28% of H–β, respectively. These results show that the β materials synthesized in a fluoride medium are

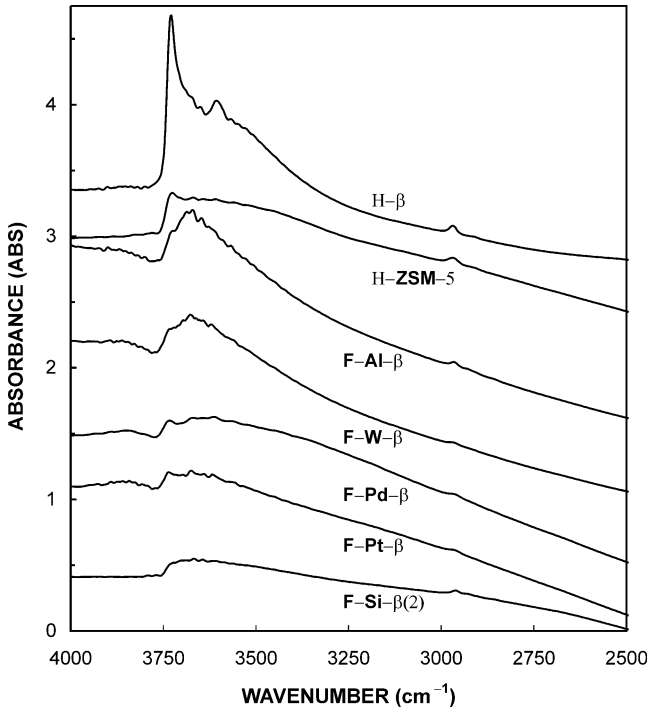

Fig. 7. Comparison of the relative coverage of surface –OH groups on various zeolites.

more hydrophobic than those synthesized in conventional ways. We can come to the conclusion that crystallization in a fluoride medium greatly decreases the number of connectivity defects in the framework of the zeolite products, further diminishing the coverage of surface hydroxyl groups, especially of isolated silanols.

3.3. Control of morphology

SEM was used to observe the morphology of various zeolite crystals and to detect the crystal size distributions as listed in Table 2 and displayed in Figs. 8–14. Very clearly, the crystal sizes of β zeolites synthesized in a fluoride medium are much larger than those of H–β (0.3–1 μm), H–Y (0.5–2.0 μm), and H–ZSM-5 (0.5–1.2 μm) synthesized in traditional hydroxide media. F–Si–β(1), F–Pt–β, F–Pd–β, and F–W–β have almost similar crystal size of about 1–4 μm. The crystal size of F–Si–β(2) (7–15 μm) without seeding (Fig. 13) is much bigger than that of F–Si–β(1) (1–4 μm) induced by H–β (Fig. 9). Whereas the big crystal size of F–Al–β (8–16 μm) (Fig. 14) is a result of co-interaction by Al and F for the spontaneous nucleation and growth of beta framework in a longer crystallization period of 12 days.

The morphology of H–β (Fig. 8) is nearly a round ball with uniform crystal size. The SEM pictures of F–Si–β(1), F–W–β, F–Pt–β, and F–Pd–β look rather similar: the uniformity of the crystals is quite poor, and these samples consist of truncated square bipyramid crystals with different sizes, rodlike crystals with different diameters, and polycrystalline aggregates with irregular shapes. The morphology of

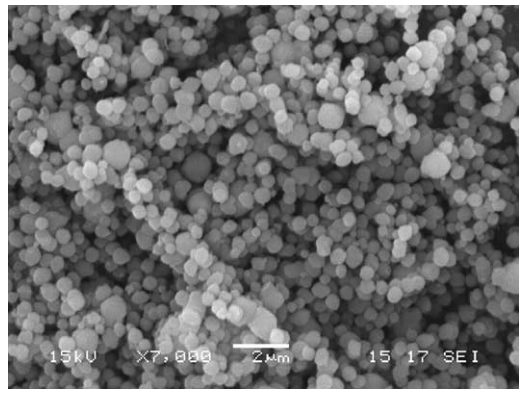

Fig. 8. SEM picture of H–β seeding crystals synthesized in an alkaline medium.

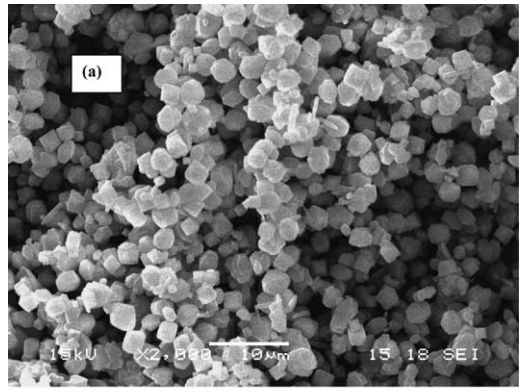

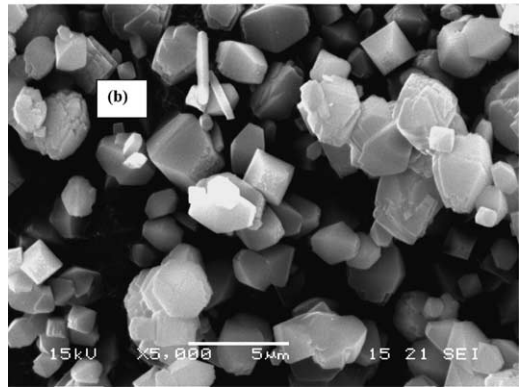

Fig. 9. SEM pictures of F–Si–β(1) synthesized with H–β seeding of 0.39 wt%: (a) full view and (b) local amplification.

siliceous F–Si–β(1), as viewed fully (a) in Fig. 9, exhibits quite rough uniformity; however, once amplified locally (b) it looks very complicated, consisting of nonuniform crystals. As viewed fully (a′) and amplified locally (b′) in Fig. 13, the morphology of F–Si–β(2) looks very uniform and perfect in a singular shape of truncated square bipyramid in which the number of rodlike crystals and twin crystals is negligible, as reported by Hazm et al. for gallium–beta zeolite [25]. Note that F–Al–β with a morphology of symmetrically faceted truncated square bipyramid was contaminated

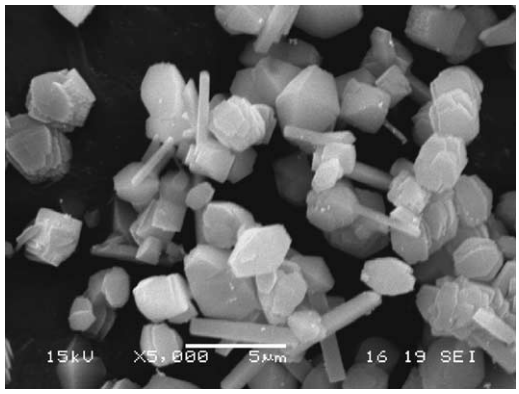

Fig. 10. SEM picture of F–Pt–β synthesized with H–β seeding of 0.40 wt%.

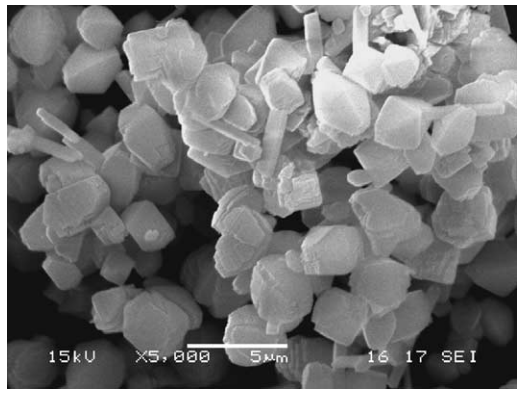

Fig. 12. SEM picture of F–W–β synthesized with seeding H–β of 0.39 wt%.

with some amorphous solid mainly consisting of noncrystallized Al species and silica as determined by EDX analysis.

The different morphologies of F–Si–$\beta(1)$ and F–Si–$\beta(2)$ have experimentally revealed the induction effect of seeding crystals on the morphology of β zeolite in a fluoride medium. The results suggest that spontaneous nucleation in a fluoride medium resulted in the formation of crystals with especially uniform crystalline morphology, while the presence of β zeolite seeding made mixed crystals consisting of different shapes. A possible formation mechanism of F–Si–$\beta(2)$ can be described below: the beta framework was spontaneously nucleated in the presence of fluoride anions, silica, and a trace amount of impurities to form numerous tiny crystal nuclei; thereafter, the soluble F-containing silica species surrounded these crystal nuclei to grow into uniformly large crystals with prolonging the crystallization time to 12 days, similar to the case of F–Al–β. However, the addition of H–β seeding largely shortened the crystallization time to 6 days and induced a relatively complicated morphology, as in the case of F–Si–$\beta(1)$, F–W–β, F–Pt–β, and F–Pd–β.

3.4. Catalytic activity in chiral hydrogenation

Tiglic acid is a simple and reactive molecule among unsaturated acids, and there is only the chiral center in the molecular configuration of hydrogenised product methylbutyric acid, which is advantageous as a model molecule. When one gas chromatograph equipped with a CP-Chirasil-L-VAL capillary column is used to analyze the reactant and products, two chirally hydrogenised products of tiglic acid, i.e., *R*-(−)- and *S*-(+)-α-methylbutyric acids, are well separated chromatographically. Prior to catalytic tests, all the Pt or Pd-containing catalysts (in Table 3) were pre-reduced at 400 °C for 10 h, and the respective metal dispersion was detected to be 35% for Pd/HZSM-5, 48% for Pd/H–β, 57% for Pd/H–Y, 65% for F–Pt–β, and 69% for F–Pd–β. Obviously, the metal dispersion on those catalysts with identical

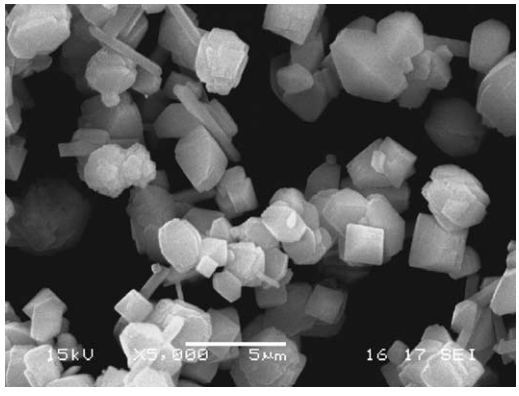

Fig. 11. SEM picture of F–Pd–β synthesized with H–β seeding of 0.40 wt%.

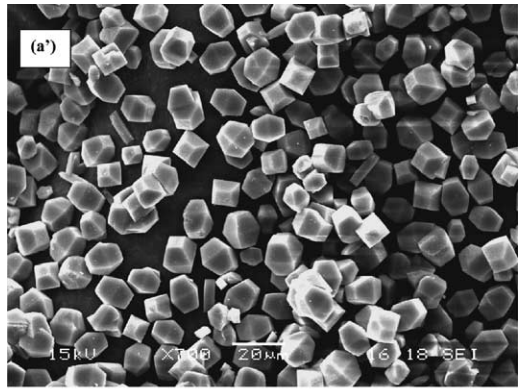

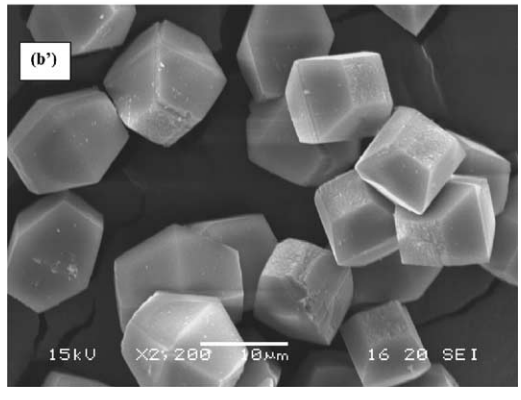

Fig. 13. SEM pictures of F–Si–$\beta(2)$ synthesized without seeding: (a′) full view and (b′) local amplification.

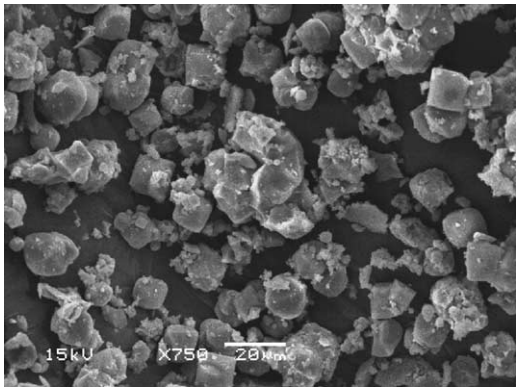

Fig. 14. SEM picture of F–Al–β zeolite synthesized without seeding.

metal contents prepared by hydrothermal synthesis is higher than that by impregnation.

For the hydrogenation of tiglic acid at room temperature in a Parr reactor, Pd/HZSM-5, Pd/H–β, and Pd/H–Y displayed good activity under H_2 pressure of 27.6 bar; however, only a racemic mixture of the hydrogenised products was acquired with an enantioselectivity (%) close to zero, implying the lack of chirality of these catalysts. F–Pt–β and F–Pd–β were highly active for the hydrogenation of tiglic acid under pressures of H_2 in which the active species for hydrogenation was Pt or Pd metals dispersed on β [41]. When F–Pt–β (reduced) was used as the catalyst, along with the increase of H_2 pressures from 13.8 to 55.2 bar, the conversion of substrate rapidly increased from 10.6 to 56.7 mol%. The TON value also displayed a gradual increase from 17.2 to 92.1 (mol of products/mol of Pt) with the increase of H_2 pressure. This is understandable because increasing the H_2 pressure increases the moles of H_2 molecules as one of the reactants, further enhancing the catalytic conversion of substrate molecules. In contrast to F–Pt–β, F–Pd–β (reduced) showed higher catalytic activity for this reaction in the range of H_2 pressures from 13.8 to 55.2 bar. At a low H_2 pressure of 13.8 bar, after 10 h about 46.5 mol% of tiglic acid could be converted. When the H_2 pressure was increased to 27.6 bar, the conversion was elevated to 82.6 mol%. Further increase in the pressure of H_2 to 41.4 bar or higher led to one 100 mol% conversion of tiglic acid. The TON value also showed a remarkable increase from 74.8 to 161.0 (mol of products/mol of Pd). The notable difference in catalytic activity of F–Pt–β and F–Pd–β for the hydrogenation of tiglic acid may be due to one fact, that the capability of palladium metal for the adsorption and decomposition of molecular hydrogen is much stronger than that of platinum metal [41]. Comparatively, under identical H_2 pressure the TON value and conversion of catalysts exhibit a decrease in the following order: F–Pd–β > Pd/H–β ≈ Pd/H–Y > Pd/HZSM-5 > F–Pt–β.

Interestingly, when F–Pt–β and F–Pd–β catalysts were applied in the hydrogenation of tiglic acid, about 9–11% e.e. value was directly obtained without the addition of chiral modifier (Table 3), in which *R*-(−)-enantiomer was dominant, further showing the chirality of pore channels of β zeolite synthesized in a fluoride medium. This very low e.e. value indicates a low-purity chirality of β channel structure, as proven by XRD patterns and other characterizations. As expected, in the reaction system consisting of Pd/HZSM-5 and F–Si–β an extremely low e.e. value of about 3.4% was achieved. However, this might not indicate a possible effect of selective adsorption of one of the products in the pores of the asymmetric zeolite in the reaction mixture, but could be an effect of a chiral modifier imposed by F–Si–β the most. For the F–Pt–β and F–Pd–β catalysts, the e.e. values were changing in the range of 8.9–11.0%. And when F–Pd–β was re-used under H_2 pressure of 27.6 bar, the e.e. value stayed more or less constant (about 10.4%) with an 82.6 mol% conversion. Considering the rigid structure of β zeolite and its recyclable and regenerable characteristics, thus, this is of rather significance, as it opens up a possibility of synthesizing the recoverable chiral porous solid catalysts in the future, which has been pursued by synthesis chemists.

4. Conclusions

A series of beta zeolite materials, such as F–Si–β, F–Pt–β, F–Pd–β, F–W–β, and F–Al–β, has been crystallized from a fluoride medium in the presence or absence of H–β seeding and characterized by different techniques. XRD patterns suggested that the stacking probability in the F–Si–β, F–Pt–β, F–Pd–β, and F–W–β materials was lower than the usual value of 0.6, i.e., the majority of these materials consisted of polymorph A with chiral structure. The chiral siliceous β framework has been proven to be free of the connectivity defects by ^{29}Si MAS NMR. The IR vibration spectra showed that synthesis in a fluoride medium could result in a higher resolution of all vibration environments of framework elements. The BET surface area and pore volume of all β samples decreased in the following order: H–β > F–Si–β(1) > F–Si–β(2) > F–Pd–β > F–Pt–β ≈ F–W–β > F–Al–β. Interestingly, for F–W–β, F–Pt–β, and F–Pd–β a visible mesoporous size distribution at 17.4–17.9 Å was detected.

The relative coverage of surface –OH groups showed a gradual reduction in the following sequence: H–β > H–ZSM-5 > F–Al–β > F–W–β > F–Pd–β > F–Pt–β > F–Si–β(1) > F–Si–β(2). Spontaneous nucleation in a fluoride medium resulted in the formation of crystals with especially uniform crystalline morphology, while the presence of H–β zeolite seeding made mixed crystals consisting of different shapes. Pd/HZSM-5, Pd/H–β, Pd/H–Y, F–Pt–β, and F–Pd–β were catalytically active for the hydrogenation of tiglic acid in the range of H_2 pressures from 13.8 to 55.2 bar; however, for this reaction an appreciable e.e. value of 9–11% was merely achieved over the F–Pt–β and F–Pd–β catalysts, without the addition of chiral modifiers, further showing the low-purity chirality of pore channels of β zeolite synthesized in a fluoride medium.

Table 3
Catalytic activity of F–Pt–β, F–Pd–β, and other Pd-containing catalysts for the chiral hydrogenation of tiglic acid

Catalyst	Metal dispersion	Hydrogen pressure	Conversion	TON[a]	Selectivity (%)		e.e.
	(%)	(bar)	(mol%)		*S*-(+)	*R*-(−)	(%)
Pd/HZSM-5	35	27.6	68.7	105.9	–	–	0
Pd/H–β	48	27.5	78.4	120.9	–	–	0
Pd/H–Y	57	27.6	76.9	118.6	–	–	0
F–Si–β + Pd/HZSM-5		27.5	65.5	101.0	48.3	51.7	3.4
F–Pt–β	65	13.8	10.6	17.2	45.5	54.4	8.9
		27.6	32.1	52.1	45.4	54.6	9.2
		41.4	50.2	81.6	45.5	54.5	9.0
		55.2	56.7	92.1	45.3	54.7	9.4
F–Pd–β	69	13.8	46.5	74.8	44.8	55.2	10.4
		27.6	82.6	133.0	44.9	55.1	10.2
		41.4	100	160.9	44.5	55.5	11.0
		55.2	100		44.7	55.3	10.6
1st[b]		27.6	82.6	133.0	44.9	55.1	10.2
2nd		27.5	83.1	133.8	44.7	55.3	10.6
3rd		27.4	82.8	133.3	44.7	55.2	10.5
4th		27.6	82.7	133.1	44.8	55.2	10.4

Redistilled methanol was used as the solvent, and reactions were carried out at room temperature for 10 h.
[a] TON equals (mol of products/mol of Pt or Pd in the catalysts).
[b] Number of recycles of the catalyst F–Pd–β.

References

[1] M.M.J. Treacy, J.M. Newsam, Nature 332 (1988) 249.
[2] J.B. Higgins, R.B. LaPierre, J.L. Schlenker, A.C. Rohrman, J.D. Wood, G.T. Kerr, W.J. Rohrbaugh, Zeolites 8 (1988) 446.
[3] M.A. Camblor, A. Corma, A. Martinez, J. Perez-Pariente, J. Chem. Soc. Chem. Commun. (1992) 589.
[4] L.L. Murrell, R.A. Overbeek, US Patent 6,004,527.
[5] T. Takewaki, S.H. Hwang, H. Yamashita, M.E. Davis, Micropor. Mesopor. Mater. 32 (1999) 265.
[6] L. Boretto, M.A. Camblor, A. Corma, J. Perez-Pariente, Appl. Catal. 82 (1992) 37.
[7] I. Kiricsi, C. Flego, G. Pazzuconi, W.O. Parker, R. Millini, C. Perego, G. Bellussi, J. Phys. Chem. 98 (1994) 4627.
[8] R.J. Taylor, R.H. Petty, Appl. Catal. A 119 (1994) 121.
[9] A. Corma, A. Martinez, P.A. Arroyo, J.L.F. Monteiro, E.F. Sousa-Aguiar, Appl. Catal. A 142 (1996) 139.
[10] H.P.R. Hari Prasad Rao, K. Ueyama, M. Matsukata, Appl. Catal. A 166 (1998) 97.
[11] Q.H. Xia, X. Chen, T. Tatsumi, J. Mol. Catal. A: Chem. 176 (2001) 179.
[12] E.G. Derouane, G.J. Hutchings, W.F. Mbafor, S.M. Roberts, New J. Chem. 8 (1998) 797.
[13] R. Kumar, A. Thangaraj, R.N. Bhat, P. Ratnasamy, Zeolites 10 (1990) 85.
[14] R.B. Borade, A. Clearfield, Microporous Mater. 2 (1994) 167.
[15] J.C. van der Waal, M.S. Rigutto, H. van Bekkum, J. Chem. Soc. Chem. Commun. (1994) 1241.
[16] M. Chatterjee, D. Bhattcharya, H. Hayashi, T. Ebina, V.Y. Onodera, T. Nagase, S. Sivasanker, T. Iwasaki, Micropor. Mesopor. Mater. 20 (1998) 87.
[17] M.A. Camblor, J. Perez-Pariente, V. Fornes, Zeolites 12 (1992) 280.
[18] M.L. Occelli, H. Eckert, A. Wolker, A. Auroux, Micropor. Mesopor. Mater. 30 (1999) 219.
[19] T. Tatsumi, Q.H. Xia, N. Jappar, Chem. Lett. (1997) 677.
[20] P. Caullet, J.E. Hazm, J.L. Guth, J.F. Joly, J. Lynch, F. Raatz, Zeolites 12 (1992) 240.
[21] S. Kallus, J. Patarin, P. Caullet, A.C. Faust, Microporous Mater. 10 (1997) 181.
[22] M.A. Camblor, A. Corma, S. Valencia, Chem. Commun. (1996) 2365.
[23] M.A. Camblor, A. Corma, S. Valencia, J. Mater. Chem. 8 (1998) 2137.
[24] T. Blasco, M.A. Camblor, A. Corma, P. Esteve, J.M. Guil, A. Martinez, J.A. Perdigon-Melon, S. Valencia, J. Phys. Chem. B 102 (1998) 75.
[25] J.E. Hazm, P. Caullet, J.L. Paillaud, M. Soulard, L. Delmotte, Micropor. Mesopor. Mater. 43 (2001) 11.
[26] J.T. Wehrli, A. Baiker, D.M. Monti, H.U. Blaser, H.P. Jalett, J. Mol. Catal. 57 (1989) 245.
[27] H.U. Blaser, H.P. Jalett, D.M. Monti, A. Baiker, J.T. Wehrli, Stud. Surf. Sci. Catal. 67 (1991) 147.
[28] J.T. Wehrli, A. Baiker, D.M. Monti, H.U. Blaser, J. Mol. Catal. 49 (1989) 195.
[29] W. Reschetilowski, U. Bohmer, J. Wiehl, Stud. Surf. Sci. Catal. 84 (1994) 2021.
[30] A. Corma, M. Iglesias, C. Pino, F. Sanchez, Stud. Surf. Sci. Catal. 75 (1993) 2293.
[31] A. Tungler, T. Tarnai, T. Mathe, J. Petro, J. Mol. Catal. 67 (1991) 277.
[32] A. Tungler, T. Tarnai, A. Deak, S. Kemeny, A. Gyori, T. Mathe, J. Petro, Stud. Surf. Sci. Catal. 78 (1993) 99.
[33] P. Papaefthimiou, T. Ioannides, X.E. Verykios, Appl. Catal. B 13 (1997) 175.
[34] R.N. Bhat, R. Kumar, J. Chem. Technol. Biotechnol. 48 (1990) 453.
[35] M.A. Camblor, A. Corma, A. Mifsud, J. Perez-Pariente, S. Valencia, Stud. Surf. Sci. Catal. 105 (1997) 341.
[36] C.A. Fyfe, H. Ströbl, G.T. Kokotailo, C.T. Pasztor, G.E. Barlow, S. Bradley, Zeolites 8 (1988) 132.
[37] K.S.W. Sing, D.H. Everett, R.A.W. Haul, L. Moscou, R.A. Pierotti, J. Rouquerol, T. Siemieniewska, Pure Appl. Chem. 57 (1985) 603.
[38] M.A. Camblor, A. Corma, S. Valencia, Micropor. Mesopor. Mater. 25 (1998) 59.
[39] J. Klinowski, M.W. Anderson, J.M. Thomas, J. Chem. Soc. Chem. Commun. (1983) 525.
[40] A. Jentys, N.H. Pham, H. Vinek, J. Chem. Soc. Faraday Trans. 92 (1996) 3287.
[41] P.N. Rylander, in: Catalytic Hydrogenation in Organic Syntheses, Academic Press, New York, 1979, p. 82.